From Light-Front Wave Functions to Parton Distribution Functions

Eduardo Pereira de Oliveira Bento Ferreira
Under supervision of Dr. Gernot Eichmann and Prof. Dr. Alfred Stadler

Departamento de Física, Instituto Superior Técnico, Lisboa, Portugal
LIP - Laboratório de Instrumentação e Física Experimental de Partículas, Lisboa, Portugal

November, 2021

Abstract

We propose a new method to calculate the valence light-front wavefunction of a system of two interacting particles. It is based on the use of the contour deformation method for the solution of the Bethe-Salpeter equation, combined with analytic continuation methods for the projection of the obtained Bethe-Salpeter wavefunction to the light-front. In this proof-of-concept study, we employ a scalar toy model and find excellent agreement between the results obtained with the new contour deformation method and the Nakanishi method used in the literature. We also demonstrate that the contour deformation method is able to handle two extensions to the scalar model that mimic some features that might be present in future applications of this method to Quantum Chromodynamics.

I Introduction

Understanding hadrons has been one of the major undertakings of modern physics. Hadrons are composed of strongly interacting quarks and gluons described by Quantum Chromodynamics (QCD) and make up almost all of the visible matter in the universe.

Even though they are very abundant, there are still many questions about their properties, namely how momentum and spin is distributed among the partons — the particles that make a hadron. Many experiments have explored these matters, for instance at HERA, RHIC and the LHC, while new ones are proposed and in construction, such as the EIC at the Brookhaven National Laboratory [1] and COMPASS/AMBER at CERN [2].

These experiments probe the partons inside the hadrons at lightlike distances and encode their spatial, momentum, spin and flavor structure. In this work, we focus on one of them: the parton distribution functions (PDFs), which can be extracted form deep inelastic scattering (DIS), which is studied in highly energetic $e^- N$ scattering experiments [3].

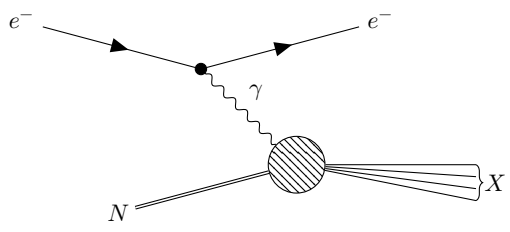

Figure 1: Schematic diagram of a Deep Inelastic Scattering event

The PDF $f_i(x, Q^2)$ is the probability distribution for a parton of species i to carry a fraction x of the total longitudinal momentum of the hadron, at some energy scale Q^2 [4]. These functions are very important in the description of the hadronic interaction with other particles.

Apart from the knowledge obtained from experiments, there have also been theoretical efforts in the calculation of the PDFs (and other structure functions) from Lattice QCD [5–7] and from continuum methods like the ones based on the Nakanishi representation [8–12].

Theoretically, the PDFs are defined on the light-front, by a specific overlap of the light-front wavefunctions (LFWFs) of the hadron [13]. In the light-front, the hadron state can be expanded in definite particle number Fock states, whose coefficients are the LFWFs [8]. To calculate the LFWFs, one needs to project the hadronic Bethe-Salpeter wavefunction (BSWF), which is the result of the bound-state equation in QCD — the Bethe-Salpeter equation (BSE), onto the light-front.

One way of performing this calculation is via the Nakanishi representation, which defines a smooth weight function g to derive the BSWF and the LFWF to handle the numerical complications brought by the analytic structure of the interaction [8, 9]. This method requires the knowledge of the full complicated analytic structure of the problem, which might not be available in practical QCD calculations. A review of other methods is given in [14].

Here we present a new method based on contour deformations which calculates the BSWF directly from the BSE while dealing with the analytic structure by deforming the needed integration paths such that the singularities are avoided [15]. The information which is needed from the BSWF to define the LFWF is then extrapolated from the BSE result through analytic continuation methods.

We first use a scalar toy model as a proof-of-concept, comparing the results obtained with the contour deformations to the Nakanishi method to demonstrate its validity.

This work begins with a brief overview of the needed theory of bound states in quantum field theory, followed by an overview of light-front dynamics and a description of the Nakanishi method and the contour deformation method. Afterwards, the obtained results are presented.

We finish with the introduction of two modifications to the scalar model that will help to bridge the gap for future QCD calculations and demonstrate that the contour deformation method is also capable of handling them.

II Bound states

II.A Bethe-Salpeter Wavefunction

The study of bound states in quantum field theories starts with the observation that the correlation functions $G(p_1, \dots, p_n)$ of the theory will produce poles when $P^2 \to m_\lambda^2$, where m_λ^2 is the squared mass of the λ state. For example, in a four-body correlation function, G factorizes to [16]:

$$G(P^2 \to m_\lambda^2) = \frac{i\Psi(\{x_i\}, P)\Psi^\dagger(\{y_i\}, P)}{P^2 - m_\lambda^2 + i\epsilon} + \text{finite terms}. \tag{1}$$

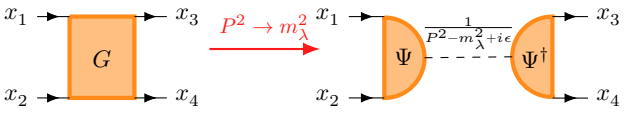

Figure 2: Schematic view of the appearance of poles and of the BSWF in correlation functions in the limit $P^2 \to m_\lambda^2$.

The residues of the poles in G are the Bethe-Salpeter WFs Ψ [17], which can be viewed as the relativistic field theory analogs of the wavefunctions of the Schrödinger equation, in non-relativistic quantum mechanics. The Bethe-Salpeter WF does not carry a probability interpretation, however, as finite-dimensional representations of the Poincaré group are not unitary.

Poincaré covariance implies that translation operators only induce a global phase factor. In the BSWF, after removing the phase factor, the remainder can be written as:

$$\Psi(x, P) = \langle 0 | \, \mathrm{T}\phi(0)\phi^*(x) \, | P \rangle \,, \tag{2}$$

$$\Psi(q, P) = \int d^4x e^{iq\cdot x} \Psi(x, P). \tag{3}$$

The calculation of the Bethe-Salpeter WFs proceeds through the analog of the Schrödinger equation in relativistic quantum field theory: the Bethe-Salpeter equation [17]. The focus of this work is the two-particle BSE, which can be written as follows (with implicit integrations over the loop momentum on the right-hand side of both equations):

$$\Psi = G_0 K \Psi \quad \Leftrightarrow \quad \psi = K G_0 \psi. \tag{4}$$

The Bethe-Salpeter amplitude ψ is defined such that $\Psi = G_0\psi$. A diagramatic representation is shown in figure 3.

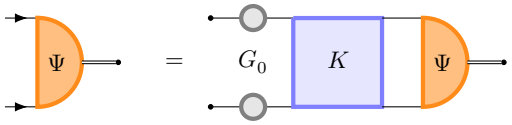

Figure 3: Schematic picture of the Bethe-Salpeter Equation

The BSE depends on two main ingredients:

- G_0, which is the product of the disconnected propagators of the two particles. These are the dressed propagators, that is, the ones with quantum corrections resulting from the quantum equations of motion - the Dyson-Schwinger equations [18, 19].
- K, which is the interaction kernel with all irreducible 2-particle diagrams — that is, the ones that do not fall apart by cutting one quark and anti-quark line.

Equation (4) amounts to an eigenvalue equation for Ψ, with an eigenvalue equal to one. In practice, one adds an artificial eigenvalue $\lambda(P^2)$ which depends on the total momentum:

$$\lambda(P^2)\psi = K G_0 \psi. \tag{5}$$

The mass of the bound state is then determined by the condition $\lambda(P^2 \to m^2) = 1$. Other excited states can be found in the same way, by obtaining the eigenvalue spectrum $\lambda_i(P^2)$ and finding the points $P_i^2 = m_i^2$ where $\lambda(P_i^2 = m_i^2) = 1$.

II.B Light-front Wavefunction

As discussed in section I, the PDFs can be calculated via the overlap of light-front WFs, which are projections of the Bethe-Salpeter WFs onto the light-front. To do so, in light-front dynamics quantities are defined on an hypersurface which is determined by [20]:

$$x^0 + x^3 = 0, \tag{6}$$

assuming a Minkowski four-vector $x^\mu = (x^0, x^1, x^2, x^3)$ and the usual metric signature $(+,-,-,-)$. One defines the light-front coordinates x^+ and x^- as

$$x^+ = x^0 + x^3, \qquad x^- = x^0 - x^3, \tag{7}$$

so that equation (6) amounts to $x^+ = 0$. The two remaining coordinates $x_\perp = \{x_1, x_2\}$ are transverse to the surface.

A four-momentum integration changes to:

$$\int d^4q = \frac{1}{2} \int d^2q^\perp \int dq^+ \int dq^-. \tag{8}$$

Using light-front dynamics has some advantages. It can be shown that in light-front dynamics, $p^- \geq 0$ implies $p^+ \geq 0$ for physical states. The vacuum $|0\rangle$ only contains $p^+ = 0$ states, in contrast to the equal-time case where $|0\rangle$ is an infinite sum of definite particle number states [9].

The simpler vacuum allows one to write hadronic states as a sum of definite particle number states. The coefficients of the said sum are the n-particle wavefunctions $\Psi_{LF}^{(n)}$, which have a probabilistic interpretation. The minimal particle number wavefunctions are the leading terms in the expansion and are known as the light-front valence WF $\Psi_{LF}^{(2)}$[8, 9].

One can now focus on the two-body valence WF and drop the superscript (2).

Taking the Bethe-Salpeter WF $\Psi(q, P)$ as a function of the total momentum $P$and the relative momentum q between the particles, the light-front WF is defined as its Fourier transform with respect to q^-, up to a normalization factor $\mathcal{C}$:

$$\Psi_{LF}(\alpha, k_\perp) = \\ = \mathcal{C} \int dq^- \Psi\left(q-, q+ = \frac{\alpha}{2}P^+, q_\perp = k_\perp, P\right), \tag{9}$$

The k^+ component is written as a fraction $\frac{\alpha}{2}$ of the P^+ component,

with $\alpha \in [-1, 1]$ which will be related to the longitudinal momentum fraction below.

One further defines the parton distribution amplitude (PDA) $\phi(\alpha)$ through an integration over $k_\perp$:

$$\phi(\alpha) = \int d^2k_\perp \Psi_{LF}(\alpha, k_\perp). \tag{10}$$

III Calculation of Light-Front Wavefunctions

III.A Euclidean conventions

In the remainder of this text, Euclidean conventions are used, which amounts to a change of the metric to $(+,+,+,+)$. This transformation is done by defining a new coordinate $x^4 = ix_0$ such that a generic four-vector x can be written as follows, with square brackets denoting Euclidean vectors from now on:

$$x = \left[x^1, x^2, x^3, x^4\right]. \tag{11}$$

As a consequence, scalar products, acquire a minus sign when compared with their Minkowski counterpart,

$$p \cdot q = -p_E \cdot q_E, \tag{12}$$

where $p_E \cdot q_E$ is related to the light-front coordinates through

$$p_E \cdot q_E = p_\perp \cdot q_\perp - \frac{1}{2}\left(x^- y^+ + x^+ y^-\right). \tag{13}$$

A four-vector x_E is spacelike if $x_E^2 > 0$ and timelike if $x^2 < 0$. On mass-shell particles have $p_E^2 = -m^2$. From now on, the subscript E is dropped.

III.B Scalar toy model

For this study, a scalar toy model will be used. It contains two scalar particles, a particle ϕ of mass m and a particle χ of mass μ. The model is defined by a very simple interaction Lagrangian:

$$\mathcal{L}_{int} = g\phi\phi\chi. \tag{14}$$

The coupling constant g has a mass dimension. Two dimensionless variables can be defined so that the mass scale m drops out of the calculations, a coupling strenght c and a mass ratio β:

$$c = \frac{g^2}{(4\pi m)^2}, \qquad \beta = \frac{\mu}{m}. \tag{15}$$

To write down the Bethe-Salpeter equation for this model two approximations are made:

- In principle, G_0 from section II.A is constructed from the particles' propagators which are obtained by solving their Dyson-Schwinger equation. In this model the dressing effects are assumed small enough so that the tree-level propagators are a good approximation [15].

- The interaction kernel K is taken to be a single ladder exchange - that is, two ϕ particles interact by exchanging a χ particle. For $\beta \to 0$ this model is known as the Wick-Cutkosky model, which has an analytical solution [21, 22].

The Bethe-Salpeter equation for the amplitude ψ is written explicitly as:

$$\psi(q, P) = \int \frac{d^4q'}{(2\pi)^4} K(q, q') G_0(q', P) \psi(q', P), \tag{16}$$

where the kernel K and G_0 can be written respectively as:

$$K(q, q') = \frac{g^2}{(q - q')^2 + \mu^2}, \tag{17}$$

$$G_0(q, P) = \frac{1}{q_1^2 + m^2} \frac{1}{q_2^2 + m^2}. \tag{18}$$

P is the total momentum, q is the external relative momentum and q' is the loop momentum. In view of the light-front dynamics to be implemented shortly, an additional vector k with $k^+ = 0$ is defined [8, 9]:

$$q = k + \left(\xi - \frac{1+\varepsilon}{2}\right) P, \tag{19}$$

$$q_1 = q + \frac{1+\varepsilon}{2} P = k + \xi P, \tag{20}$$

$$q_2 = -q + \frac{1-\varepsilon}{2} P = -k + (1-\xi) P. \tag{21}$$

Here, $\varepsilon \in [-1, 1]$ is an arbitrary momentum partitioning parameter and $\xi \in [0, 1]$ is the longitudinal momentum fraction. A comparison with equation (9) shows that

$$q_1 = \xi P^+, \qquad q_2 = (1-\xi) P^+, \qquad \xi = \frac{1+\alpha}{2}, \tag{22}$$

that is, the particles carry a fraction ξ and $(1-\xi)$, respectively, of the longitudinal momentum P^+ of the bound state.

III.C Nakanishi Method

From the definitions of K and G_0 in equations (17) and (18), respectively, one can see that there are singularities that require attention when performing the calculations numerically.

One method to avoid these complications is based on the Nakanishi method [23]. The main idea is to represent the Bethe-Salpeter WF as an integral over a non-singular weight-function - the *Nakanishi weight function* - multiplied by a denominator that carries the analytic structure. The desired quantities such as the light-front WF and the PDA are then extracted from the weight function.

The light-front WF can then be written as an integral over the weight function [8, 9]:

$$\Psi_{LF}(x, z) = \frac{1}{4\sqrt{2}} \int_0^\infty dx' \frac{(1-z^2)^2 h(x', z)}{\left[x' + x + 1 + t(1-z^2)\right]^2}. \tag{23}$$

To access all these quantities it is first necessary to determine the weight function h from the Bethe-Salpeter equation, now as an equation for h:

$$\int_0^\infty dx' \frac{h(x',z)}{\left[x'+\mathcal{N}(x,z)\right]^2} = \int_0^\infty dx' \int_{-1}^1 dz' V(x,z,x',z') \frac{1-z'^2}{1-z^2} h(x',z'), \tag{24}$$

$$\mathcal{N}(x,z) = x+1+t(1-z^2), \tag{25}$$

$$V(x,z,x',z') = \frac{c}{2}\frac{1}{\mathcal{N}(x,z)} \int_0^1 dv \left[K(v,z,z',x,x') + K(v,-z,-z',x,x')\right], \tag{26}$$

$$K(v,z,z',x,x') = \frac{\theta(z'-z)(1+z)^2 v^2}{\left[v(1-v)(1+z')\mathcal{N}(x,z) + v^2(1+z)\mathcal{N}(x',z') + (1-v)(1+z)(\beta+vx')\right]^2}. \tag{27}$$

To calculate the light-front WF from the Nakanishi method it is necessary to know the full details of the analytic structure of the ingredients. In practical dynamical calculations, this may not be the case.

III.D Contour deformations

The method proposed in this work tries to overcome these difficulties by integrating equation (16) directly, and dealing with the analytic structure by avoiding the singularities through deformations of the integration path [15].

In the case of the scalar toy model, the locations of the singularities are already known. In principle one only needs to know the integration regions that are free of singularities so that the integration path can be deformed, allowing its application to problems where this information is only available, for example, numerically.

The first step in this method is to define the kinematics of the problem, based on the definitions of III.B. The rest frame of the hadron will be used as reference, thus writing P and k:

$$P = 2m\sqrt{t}\begin{bmatrix}0\\0\\0\\1\end{bmatrix}, \qquad k = m\sqrt{x}\begin{bmatrix}0\\0\\\sqrt{1-\omega^2}\\\omega\end{bmatrix}. \tag{28}$$

The condition $k^+ = 0$ will be implemented later when projecting the Bethe-Salpeter WF onto the light-front. Equation (28) defines the following three Lorentz invariants:

$$x = \frac{k^2}{m^2}, \qquad \omega = \hat{k}\cdot\hat{P}, \qquad t = \frac{P^2}{4m^2}, \tag{29}$$

and $P^2 = -M^2$, with M is the mass of the bound state.

In the following analysis, the parameter η is taken to be $\eta = \frac{1}{2}$. According to equation (22), the light-front momentum partitioning parameter $\alpha = 2\xi - 1$ is introduced, such that:

$$q_1 = k + \left(\frac{1+\alpha}{2}\right)P, \qquad q_2 = -k + \left(\frac{1-\alpha}{2}\right)P, \tag{30}$$

and the product of the propagators, G_0, becomes

$$m^4 G_0(x,\omega,t,\alpha) = \frac{1}{(x+1+t+\alpha^2 t+2\alpha\omega\sqrt{x}\sqrt{t})^2 - 4t(\alpha\sqrt{t}+\omega\sqrt{x})^2}. \tag{31}$$

Before writing the kernel K, the loop momentum k' is expressed in hyperspherical coordinates:

$$k' = m\sqrt{x'}\begin{bmatrix}\sqrt{1-\omega'^2}\sqrt{1-y^2}\sin\vartheta\\ \sqrt{1-\omega'^2}\sqrt{1-y^2}\cos\vartheta\\ \sqrt{1-\omega'^2}y\\ \omega'\end{bmatrix}. \tag{32}$$

With these definitions, the kernel K becomes:

$$m^2 K(x,\omega,x',\omega',y) = \frac{1}{x+x'+\beta^2-2\sqrt{x}\sqrt{x'}\Omega(\omega,\omega',y)}, \tag{33}$$

$$\Omega(\omega,\omega',y) = \omega\omega' + \sqrt{1-\omega^2}\sqrt{1-\omega'^2}y. \tag{34}$$

After collecting all elements the final form of the Bethe-Salpeter equation can then be written:

$$\begin{aligned}\psi(x,\omega,t,\alpha) &= \\ &= \frac{g^2}{m^2}\frac{1}{(2\pi)^3}\frac{1}{2}\int_0^\infty dx' x' \\ &\times \int_{-1}^1 d\omega' \sqrt{1-\omega'^2} G_0(x',\omega',t,\alpha) \\ &\times \int_{-1}^1 dy\, K(x,\omega,x',\omega',y)\psi(x',\omega',t,\alpha).\end{aligned} \tag{35}$$

The integration in y can be done analytically using

$$\int_{-1}^1 dy \frac{1}{A-By} = \frac{\log(A+B)-\log(A-B)}{B}. \tag{36}$$

III.E Projection onto the light-front

To obtain the light-front WF from the calculated Bethe-Salpeter WF it is necessary to transform (9) to Euclidean kinematics.

The first step is to understand the integration in q^- in the kinematics of (28) and implement the condition $k^+ = 0$. This is done by considering k and P in a moving frame:

$$P = 2m\sqrt{t}\begin{bmatrix}0\\0\\\sqrt{1-Z^2}\\Z\end{bmatrix}, \tag{37}$$

$$k = m\sqrt{x}\begin{bmatrix}\sqrt{1-z^2}\sqrt{1-y^2}\sin\vartheta\\ \sqrt{1-z^2}\sqrt{1-y^2}\cos\vartheta\\ \sqrt{1-z^2}y\\ z\end{bmatrix}. \tag{38}$$

The momentum P gains an extra parameter Z, and the condition $k^+ = 0$ implies $y = iz/\sqrt{1-z^2}$ with $\omega = \hat{k}\cdot\hat{P}$ as in (29). This entails $\frac{k_\perp^2}{m^2} = x$ — the x variable plays the role of the transverse momentum squared. One can now write q^- as a function of the new variables:

$$q^- = -\frac{2m^2}{P^+}\left(2\sqrt{x}\sqrt{t}\omega + \alpha t\right). \tag{39}$$

For the light-front WF in (9), α, t, x are fixed and ω is the integration variable. As the original domain in q^- is $(-i\infty, i\infty)$ and $\sqrt{t} = \frac{iM}{2m}$, then $\omega \in (-\infty, \infty)$. The final form of the light-front WF, written in its dimensionless form $\tilde{\Psi}_{LF}$, is then given by

$$\tilde{\Psi}_{LF}(\alpha, x, t) = \frac{2\sqrt{x}\sqrt{t}}{i\pi}\int_{-\infty}^{\infty} d\omega\, \Psi(x, \omega, t, \alpha)|_{k^+=0}. \tag{40}$$

In the moving frame, the solution of the Bethe-Salpeter WF is $\Psi(x, z, y, Z, t, \alpha)$, where

$$\hat{k}\cdot\hat{P} = zZ + y\sqrt{1-z^2}\sqrt{1-Z^2}. \tag{41}$$

Because the Bethe-Salpeter WF is Lorentz invariant, its solution in the moving frame and in the rest frame must be the same, therefore the rest frame solution (40) can be equally used for Ψ in (9).

The Bethe-Salpeter equation, however, only provides the WF in the domain $\omega \in [-1, 1]$, so, to be able to access $\omega \in \mathbb{R}$, numerical analytic continuation methods will be used.

IV Analytic Structure

IV.A Propagators

By equating the denominator of the propagator product G_0 to zero, one can find its singularities. There are two singularities in the complex ω plane:

$$\begin{aligned}\omega_+ &= -\frac{x + 1 + (1+\alpha)^2 t}{2(1+\alpha)\sqrt{x}\sqrt{t}},\\ \omega_- &= \frac{x + 1 + (1-\alpha)^2 t}{2(1-\alpha)\sqrt{x}\sqrt{t}}.\end{aligned} \tag{42}$$

After the integration in ω, these will become cuts in the complex $\sqrt{x}$ plane. The cuts depend on α and are parametrized by the value of $\omega \in [-1, 1]$. There are four cuts, labeled by two parameters, χ and λ, that can take on the values, ± 1. The cuts have a generic form, written as:

$$\sqrt{x}^{\lambda}_{\chi} = A\sqrt{t}\left[\omega + i\lambda\sqrt{\omega^2 - 1 - \frac{1}{t(1+\chi\alpha)^2}}\right], \tag{43}$$

where the prefactor A is written as a function of χ and α:

$$A(\chi, \alpha) = \begin{cases} -(1+\alpha), & \chi = + \\ (1-\alpha), & \chi = - \end{cases}. \tag{44}$$

An example configuration of the cuts in the complex $\sqrt{t}$ plane is shown in figure 4.

To be able to do the integration without crossing any branch cuts, the path in $\sqrt{x}$ must go through the green line in figure 4 until reaching the outermost point, which, for any $\alpha \in [-1, 1]$, is given by:

$$\max\left(1+\alpha, 1-\alpha\right)\sqrt{t}. \tag{45}$$

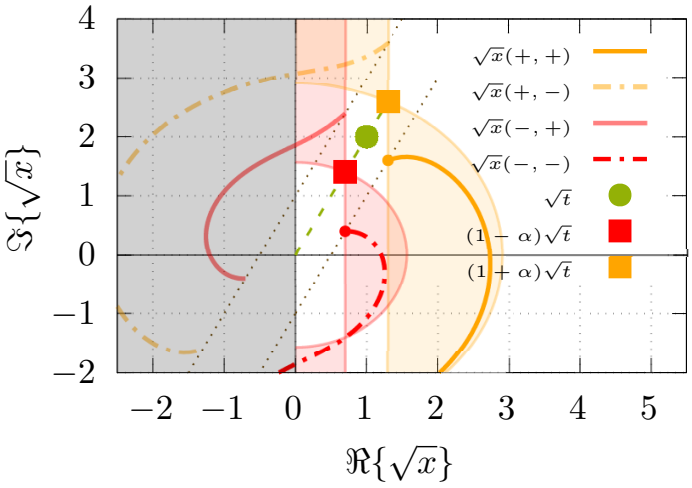

Figure 4: Branch cuts $\sqrt{x}^{\lambda}_{\chi} \equiv \sqrt{x}(\chi, \lambda)$ of G_0 in the complex $\sqrt{x}$ plane, for $\alpha = 0.3$ and $\sqrt{t} = 1 + 2i$. The real axis is intersected by one of the cuts generated by G_0 thus requiring contour deformations. The shaded areas indicate the regions of the $\sqrt{x}$ plane where there might be branch cuts.

For a purely imaginary $\sqrt{t}$, the branch cuts close on themselves, making it impossible to create a viable contour deformation. For numerical calculations, it is necessary to add a real part to $\sqrt{t}$, which amounts to working with a complex mass M.

The cuts do not cross the real axis, and therefore one can use the usual path $\sqrt{x} \in (-\infty, \infty)$ without contour deformations, if the following condition holds:

$$\Im\{\sqrt{t}\} < \frac{1}{1-\alpha} \wedge \Im\{\sqrt{t}\} < \frac{1}{1+\alpha}. \tag{46}$$

IV.B Kernel

Repeating the same proceeding as for the propagator product G_0, one can derive the branch cuts in the $\sqrt{x'}$ complex plane generated by the kernel. These cuts have a very similar structure to the propagator cuts, and can be written as

$$\sqrt{x'}_{\chi} = \sqrt{x}\left(\Omega + i\chi\sqrt{\Omega^2 - 1 - \frac{\beta^2}{x}}\right). \tag{47}$$

Following the convention of (35), the primed variable corresponds to the loop momentum and the non-primed corresponds to the external momentum.

For ω, ω' and y inside the usual range $[-1, 1]$ Ω is also bounded in the same interval $\Omega \in [-1, 1]$.

Although these cuts look very similar to the ones from the propagators, there is an additional caveat, related to the structure of the Bethe-Salpeter equation as an integral equation. In practical calculations, it is needed to iterate the obtained solution until convergence, which requires the path in the external $\sqrt{x}$ to be the same as the loop path in $\sqrt{x'}$.

But the cuts (47) in $\sqrt{x'}$ also depend on the external variable $\sqrt{x}$. A path that avoids the kernel cuts for a specific value of $\sqrt{x}$

must also avoid the cuts for all other previous values of $\sqrt{x}$. When constructing a path for the $\sqrt{x'}$ integration, one is always bounded by one vertical line and a circle, which delimit the safe region to proceed, as shown in figure 5.

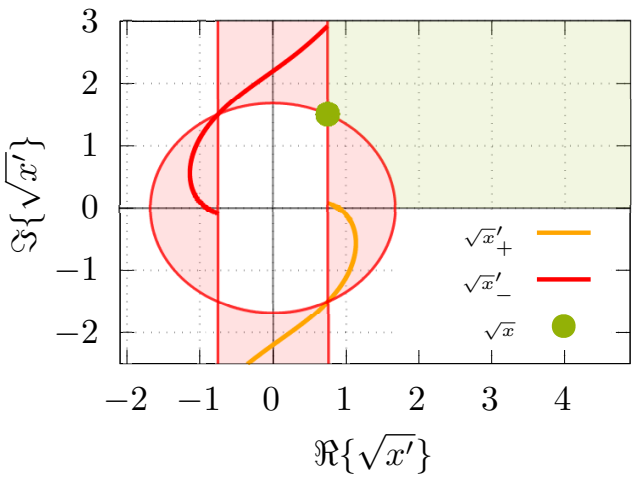

Figure 5: Kernel cuts $\sqrt{x'}_\chi$ for $\beta = 2$ and $\sqrt{x} = 1 + 2i$. The red shaded regions mark the possible locations where cuts can exist, while the green region marks a safe region for the subsequent value of $\sqrt{x}$.

The vertical line and the circle translate to the requirement that the path in $\sqrt{x'}$ must always increase in both the real part, and in the absolute value.

IV.C Integration path

The collection of the constraints from the propagators G_0 and the kernel K result in a path for the integration in $\sqrt{x'}$ that must always increase in both real part and absolute value, while also going through the green dashed line in figure 4.

One can then identify three separate segments of the integration path:

1. The first segment proceeds from the origin to the outermost point in the dashed green line of figure 4, given by (45). This outermost point will be called $\sqrt{\tau}$ in what follows.

2. The second segment returns back to the real axis, following a circle centered in the origin that increases its radius along the way, in order to comply with the requirement that the path must always increase in the absolute value.

3. Finally, the last segment connects to the previous one on the real axis and then continues to $+\infty$, with no further cuts to avoid.

One can write the three segments as three different connected paths, parametrized by one variable $z \in [-1, 1]$. The domain was selected such as to simplify the numerical implementation. The paths, named $\gamma_i(z)$ are:

$$\gamma_1(z) = \sqrt{\tau} z_+ \tag{48}$$

$$\gamma_2(z) = |\sqrt{\tau}|\,(r_{max} z_+ + z_-)\, e^{i \arg(\sqrt{\tau}) z_-}, \tag{49}$$

$$\gamma_3(z) = \frac{1 + z + 2 r_{max} |\sqrt{\tau}|}{1 - z}, \tag{50}$$

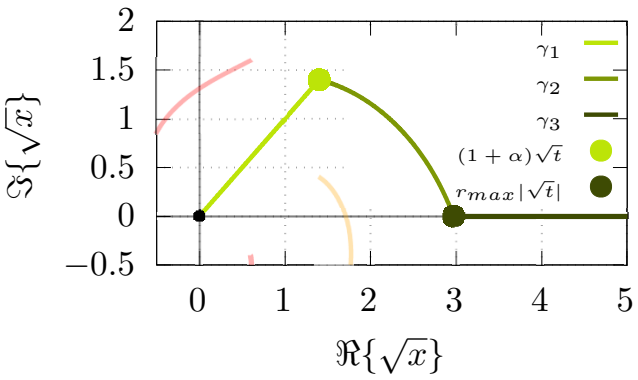

Figure 6: Integration path for $\sqrt{t} = 1 + i$, $\alpha = 0.4$ and $r_{max} = 1.5$. The red and orange lines are the propagator cuts.

$\Im\{\sqrt{t}\}$	0.20	0.80	1.20
$\Re\{1/\lambda\}$	10.815	8.694	6.341
$\Im\{1/\lambda\}$	0.267	1.431	3.853

Table 1: Inverse eigenvalue $1/\lambda$, of the Bethe-Salpeter equation, for three values of $\Im\{\sqrt{t}\}$.

where $r_{max} > 1$ to avoid the kernel cuts. The quantities z_+ and z_- are defined as:

$$z_+ = \frac{1+z}{2}, \qquad z_- = \frac{1-z}{2}. \tag{51}$$

An example path is shown in figure 6.

The integration in the $\sqrt{x}$ variable is finally written as a sum of the contribution of the three paths:

$$\int_0^\infty \mathcal{F}(x')dx' \to \sum_{i=1}^{3} \int_{-1}^{1} \gamma_i'(z) \mathcal{F}(\gamma_i(z))\, dz, \tag{52}$$

where $\gamma_i'(z)$ is the derivative of $\gamma_i(z)$ with respect to z.

V Results

In this section, the numerical results obtained from the contour deformations method are presented and compared with the results obtained from an implementation of the Nakanishi method, following section III.C.

V.A Bethe-Salpeter amplitude

This section starts with the discussion of the properties of the Bethe-Salpeter amplitude obtained from its BSE. The results discussed in the following were obtained by numerical integration with Gaussian quadrature [24], of equation (35), with $N_x = 96$ points in x and $N_\omega = 95$ points in the ω integration. Three values of $\sqrt{t} = 0.20 + 0.20i$, $0.20 + 0.80i$ and $0.20 + 1.20i$, as well as $\beta = 4$ were chosen. $\alpha \in [-1, 1]$ is an external variable in the BSE.

Firstly, the focus is on the inverse eigenvalue $1/\lambda$ as in equation (5). In this work, only the ground state (highest eigenvalue) was calculated, however, it is equally possible to obtain the whole spectrum. The results are displayed in table 1.

A three-dimensional plot of the amplitude for $\sqrt{t} = 0.20 + 0.20i$ is shown in figure 7, as a function of x and ω and for a value of

$\alpha = -0.602$. Figure 7 highlights the main features of the Bethe-Salpeter amplitude. There is a strong x dependence, i.e., the amplitude falls off with x (which corresponds to $k_\perp^2$), but almost no variation in ω. Figure 8 shows the ω dependence for one value of $x = 11$ and two opposite values of α.

One can see that the Bethe-Salpeter has a symmetry under the combined transformation

$$\omega \to -\omega, \qquad \alpha \to -\alpha. \tag{53}$$

This symmetry is just a manifestation of the fact that the two constituents are indistinguishable and as such, the labeling of the momentum four-vectors q_1 and q_2 is arbitrary. Equation (53) is equivalent to relabeling the two particles.

The dependence of the Bethe-Salpeter amplitude on x is shown in figure 9. The main difference between the three values of $\sqrt{t}$ appears mainly in the imaginary part of the amplitude.

Finally, the eigenvalues of the BSE were also calculated as functions of $\sqrt{t}$, for different values of $\Re\{\sqrt{t}\}$. Figure 10 displays the results which are in perfect agreement with figure 11 of [15] and the Nakanishi results [8, 9], plotted as red dots in figure, 10 for $\Re\{\sqrt{t}\} = 0.20$.

V.B Light-front WF and PDA

After having calculated the Bethe-Salpeter amplitude ψ, we proceed to the calculation of the light-front WF via the solution of equation (40).

As discussed in section III.E, the BSE result for the amplitude ψ is only available in the domain $\omega \in [-1, 1]$, whereas the LFWF requires the knowledge of Ψ over the whole domain $\omega \in (-\infty, \infty)$. To this end, an analytic continuation using the Schlessinger point method is employed [25]. It takes N points of the target function f as input and returns an approximation R of f in the form of a

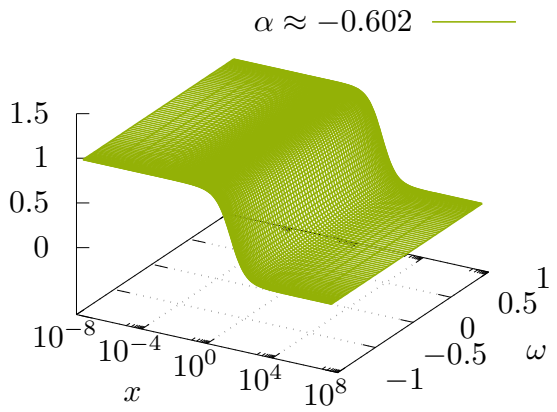

Figure 7: Bethe-Salpeter amplitude for $\sqrt{t} = 0.20 + 0.20i$, as a function of x and ω.

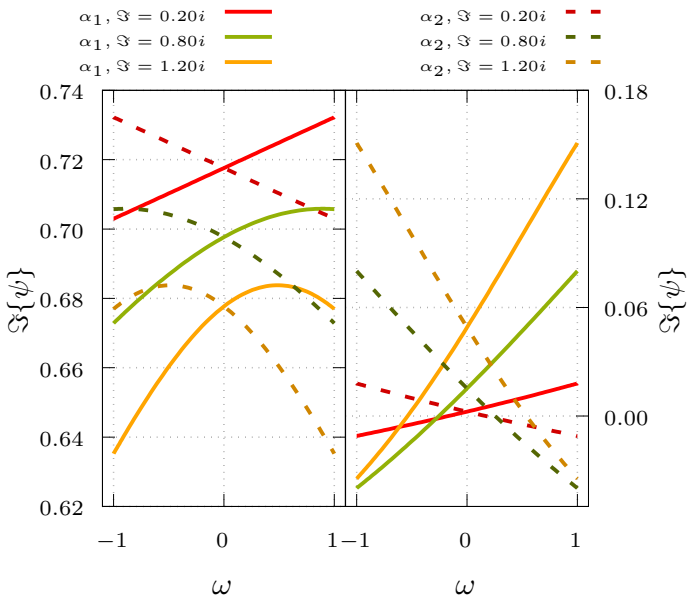

Figure 8: ω dependence of the Bethe-Salpeter amplitude ψ for $\alpha_1 = -0.602$, $\alpha_2 = 0.602$ and $x = 11$.

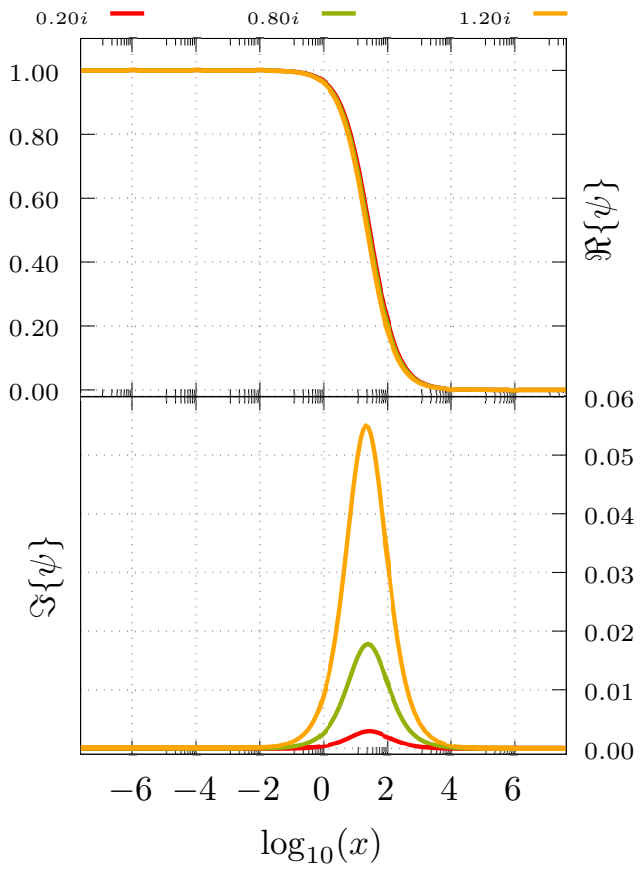

Figure 9: x dependence of the Bethe-Salpeter amplitude ψ for $\alpha_1 = -0.602$ and $x = 11$.

continued fraction:

$$R(x) = \cfrac{f(x_1)}{1 + \cfrac{a_1(x - x_1)}{1 + \cfrac{a_2(x - x_2)}{1 + \cdots}}} \tag{54}$$

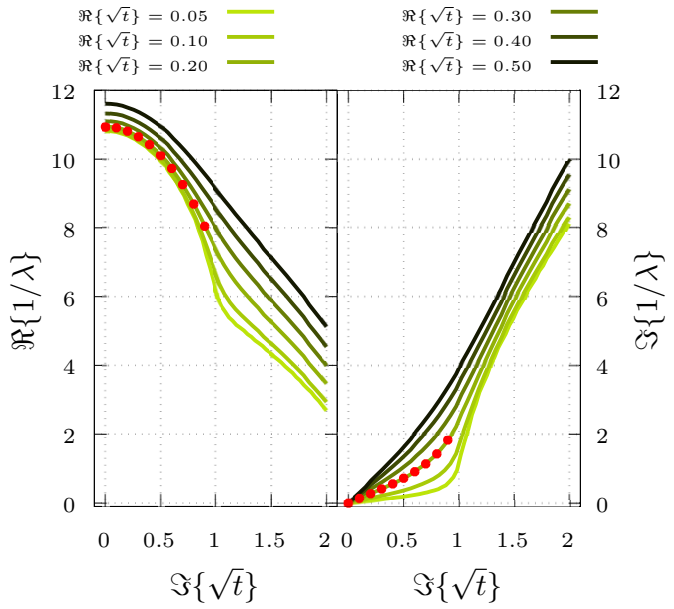

Figure 10: Eigenvalues of the Bethe-Salpeter equation as a function of $\sqrt{t}$.

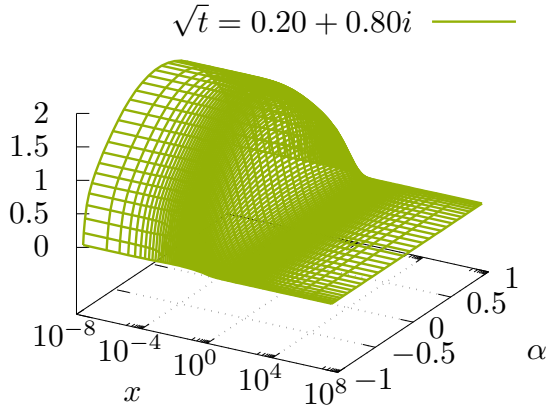

Figure 11: Absolute value of the light-front wavefunction (not normalized)as a function of x and α.

The coefficients a_i of the fraction are determined by enforcing the requirement that $R(x_i) = f(x_i)$ at the input points.

The following results for the light-front wavefunction were obtained with the Bethe-Salpeter amplitudes calculated in the previous section, and by using 24 points as input to the Schlessinger method. The Nakanishi method results used for comparison were obtained with $N_x = 40$ and $N_z = 30$. The light-front wavefunction as a function of $\sqrt{t} = 0.20 + 0.80i$ is shown in figure 11.

To allow for a comparison between the contour deformation and Nakanishi results, the light-front WFs are normalized as follows (inspired by the probabilistic interpretation as discussed in II.B):

$$1 = \int dx \int d\alpha \, \tilde{\Psi}_{LF}(x, \alpha). \tag{55}$$

Figure 11 shows all the expected features of the light-front WF: it vanishes for large values of x so that the integral over x is finite [8]. It also vanishes at the endpoints $\alpha = \pm 1$, as those cases correspond to one of the constituents having all of the longitudinal momentum of the particle. It is also symmetric in α, which is a consequence of the particle exchange symmetry of (53).

Figures 12 and 13 show the dependence of the light-front WF in x and α, respectively, as well as an overlay with the Nakanishi results for comparison.

Finally, from the calculated light-front WF we calculate the PDA $\phi(\alpha)$, which gives the probability of finding the constituents in a configuration with a given value of α.

The results are again normalized in a similar way as for the light-front WF:

$$1 = \int d\alpha \, \phi(\alpha). \tag{56}$$

Figure 14 shows the PDA results from the contour deformation method, which are in excellent agreement with the Nakanishi method. The PDAs also carry the same properties in α that were expected from the light-front WFs.

The good agreement of the results with the Nakanishi method demonstrate that it is possible to calculate light-front WFs using the contour deformation method.

VI Extensions of the scalar model

To help bridge the gap to QCD, the scalar toy model of section III.B was extended in two directions:

1. One can implement particles with unequal masses, as the different quark flavours have different masses (see [26]);

2. One can implement propagators with complex conjugate poles, (to mimic typical results for the quark propagator in a rainbow ladder truncation [16]).

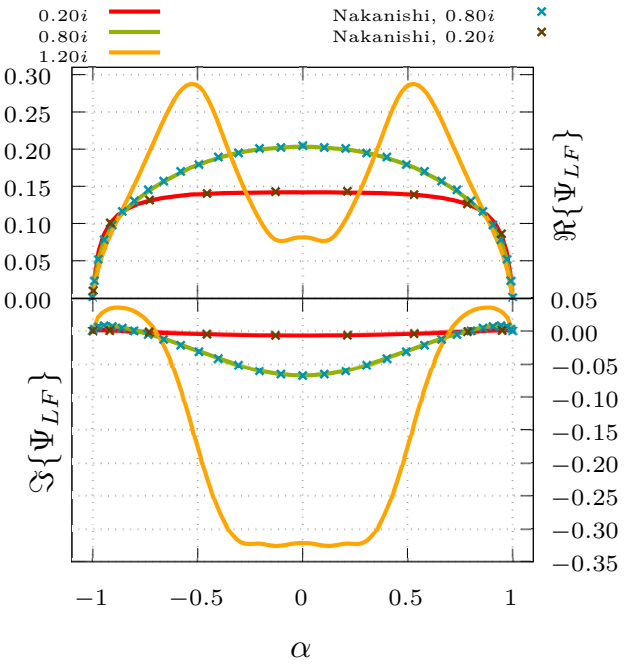

Figure 12: α dependency of the light-front WF for a fixed value of $x = 0.33$.

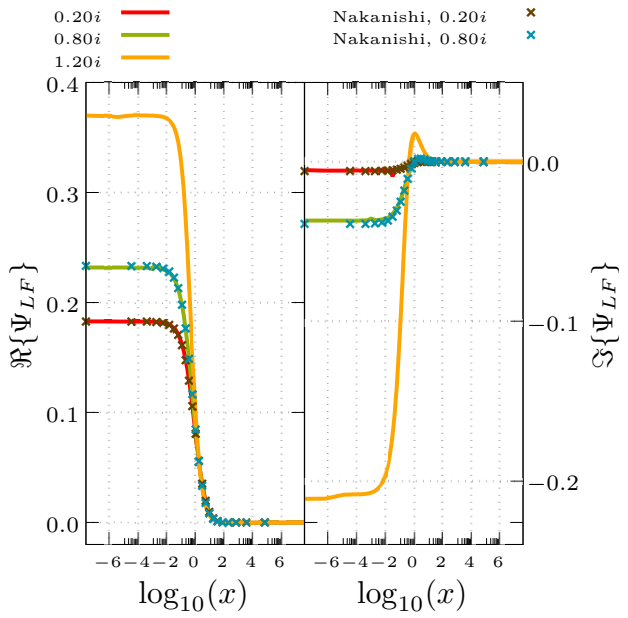

Figure 13: x dependency of the light-front WF for a fixed value of $\alpha = -0.67$.

VI.A Unequal masses

The study of this case starts with the parameter ε, whose purpose is to maximize the domain in $\sqrt{t}$. For an optimal value of

$$\varepsilon = \frac{m_1 - m_2}{m_1 + m_2}, \tag{57}$$

the $-M^2 = -(m_1+m_2)^2$ threshold is at $\sqrt{t} = 1$. Defining the mass scale $2m = m_1 + m_2$, and setting ε to the optimal value, one writes the two masses of the two particles as functions of ε and m:

$$m_1 = (1+\varepsilon)m \qquad m_2 = (1-\varepsilon)m. \tag{58}$$

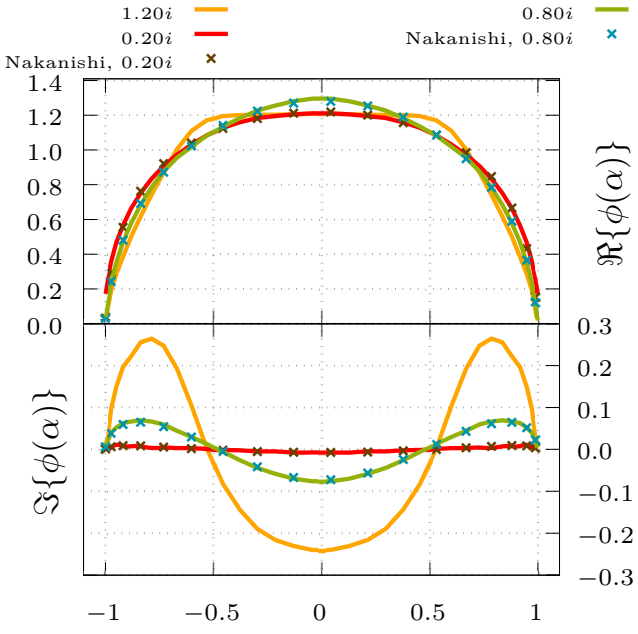

Figure 14: Calculated parton distribution amplitudes $\phi(\alpha)$.

The parameter ε sets the mass ratio and the parameter m sets the scale that can be taken out of the equations.

The kernel K of (33) does not depend on the mass, and as such remains invariant. The only difference from the equal masses case comes from the propagators G_0, which, using the definitions of (29) can be written as:

$$m^4 G_0(x,\omega,t,\alpha,\varepsilon) = \frac{1}{\left(x+1+t+\alpha^2 t+2\alpha\omega\sqrt{x}\sqrt{t}+\varepsilon^2\right)^2 - 4\left(\alpha t+\sqrt{x}\sqrt{t}\omega+\varepsilon\right)^2}. \tag{59}$$

The resulting branch cuts are the same as the ones from the equal mass case, except that there is a dependence on ε,

$$\sqrt{x}^{\lambda}_{\chi} = A(\chi,\alpha)\left[\sqrt{t}\omega + i\lambda\sqrt{t(1-\omega^2)+\left(\frac{1+\chi\varepsilon}{1+\chi\alpha}\right)^2}\right], \tag{60}$$

where all the quantities are defined as for the equal masses case.

The propagator cuts (60) are already contained in the shaded regions of figure 4 and, as such, the path of section IV.C already avoids them and can be used without modification.

With this, one can calculate the light-front WF for this model as well. The following results were calculated for five different values of $\varepsilon = \{-0.5, -0.25, 0, 0.25, 0.50\}$, and $\sqrt{t} = 0.2 + 0.8i$. The number of integration points used was $N_x = 96$ and $N_\omega = 72$.

Figure 15 shows the effect of the ε parameter. It introduces a skewness in the function, making it tilt to the side of the heavier particle, which on average has a higher fraction of the momentum. It also shows that the particle exchange symmetry now also requires switching the sign of ε.

The x dependence is similar to the equal mass case of $\varepsilon = 0$ and the PDA mirrors the information in figure 15.

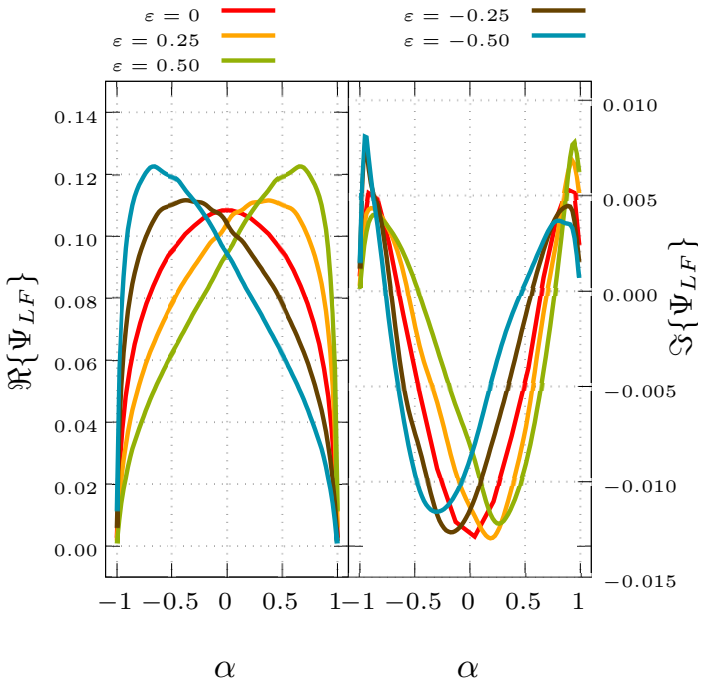

Figure 15: α dependence of the light-front WF for five values of ε.

VI.B Complex conjugate poles

In this extension, we assume that the propagators have a complex conjugate pair of mass poles of the form:

$$D_\phi(q) = \frac{1}{q^2+m^2} \longrightarrow \frac{1}{2}\left(\frac{1}{q^2+m^2} + \frac{1}{q^2+(m^*)^2}\right). \tag{61}$$

The complex mass can be written as follows, which defines a parameter δ :

$$m^2 \to m^2(1+i\delta). \tag{62}$$

Note that inverting the sign of δ has the same effect as taking the complex conjugate of the mass. As the propagator (61) is a sum of both the mass and the conjugate, it is even in δ and thus, it is sufficient to consider $\delta \geq 0$.

Again, the kernel K is invariant, and the only change happens in the propagator.

Defining Γ_Ξ as follows, with $\Xi = \{+,-\}$:

$$\Gamma_\Xi = \left(x+t+1+\alpha^2 t + 2\alpha\omega\sqrt{x}\sqrt{t}\right)^2 + 4t\Xi\left(\alpha\sqrt{t}+\omega\sqrt{x}\right)^2, \tag{63}$$

and ζ as:

$$\zeta = 4\sqrt{t}\left(\alpha\sqrt{t}+\omega\sqrt{x}\right)\left(x+t+1+\alpha^2 t+2\alpha\omega\sqrt{x}\sqrt{t}\right), \tag{64}$$

the propagator product G_0 can be written as:

$$m^4 G_0 = \frac{\Gamma_-}{\left(\Gamma_+ + \delta^2\right)^2 - \zeta^2}. \tag{65}$$

The propagators G_0 have cuts similar to the previous case, but with a δ dependence:

$$\sqrt{x}_\chi^{\{\lambda,\nu\}} = A(\chi,\alpha)\left[\sqrt{t}\omega + i\lambda\sqrt{t(1-\omega^2)+\frac{1+\nu i\delta}{(1+\chi\alpha)^2}}\right]. \tag{66}$$

There are now eight cuts, that, due to the term $i\delta$, will rotate and, for $|\delta|$ larger that a specific value δ_{crit}, the cuts overlap and prevent any contour deformation. The condition which defines the safe region in δ is:

$$\Im\{\sqrt{\tau}\} < \frac{\Im\{i\sqrt{1+i\delta}\}\Re\{\sqrt{\tau}\}}{\Re\{i\sqrt{1+i\delta}\}}. \tag{67}$$

Note that the equation (67) applies to the case $\nu = +$. For the case $\nu = -$ there is also a condition, and the safe region for δ is defined as the intersection of both. The path defined in section IV.C is still valid for this problem.

A calculation of the light-front WF and the PDAs is also possible, provided that the parameters are within the safe zone. In figure 16 the obtained PDAs are presented for three different values of δ and $\sqrt{t} = 0.2+0.8i$. For this value of $\sqrt{t}$, the safe region is $|\delta| < \frac{8}{15}$. The number of integration points used was $N_x = 128$ and $N_\omega = 96$.

Figure 16 shows that it is still possible to obtain the light-front WF and the PDA for the complex mass case, provided that care is taken to stay within the safe zone for δ. One can also see that, altough the differences between the values of δ are not very pronounced, as δ approaches the limit the numerics get worse, as the cuts get closer to the integration path in $\sqrt{x}$.

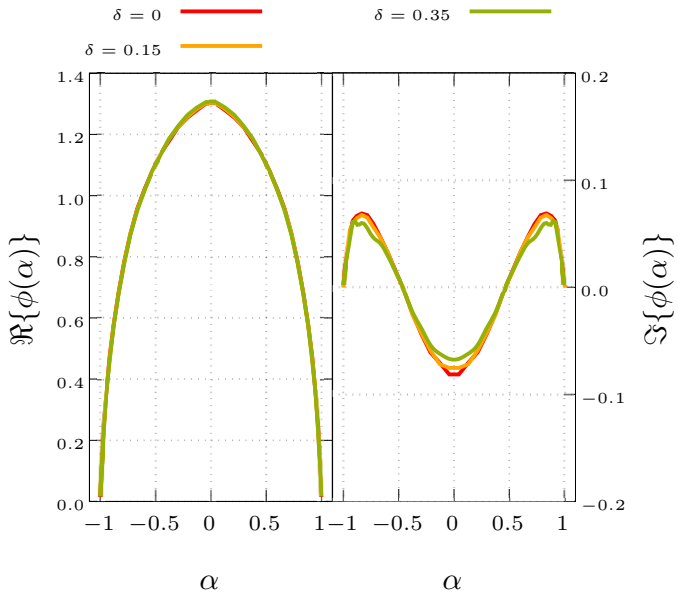

Figure 16: Plot of the calculated PDA for the complex conjugate masses case, for different values of δ.

VII Closing remarks

In this work, a new method for calculating light-front WFs was proposed. The main idea is to develop a method that is able to integrate the Bethe-Salpeter WF directly without the having to know its whole analytic structure, which might not even be possible in practical calculations of QCD.

The main hurdle in this process is the fact that the amplitude needs to be analytically continued to the entire real axis. Although very powerful, a more systematic study of the Schlessinger method might prove helpful in the numeric stability of the method.

We could, nevertheless, demonstrate that the contour deformation method is capable of calculating the light-front wave functions, and that its results are in agreement with the Nakanishi method which is well established in the community. It also has the added advantage that it can calculate resonances beyond the threshold, and it needs fewer integrations than the Nakanishi method which makes it very fast in comparison. These results open the door to future calculations of the PDFs and other quantities using the contour deformation method.

As the contour deformation method was also successful in calculating the light-front WF and the PDA for extensions of the scalar model, there is a good chance that it can be successfully applied to QCD, opening the door to calculations of a broad number of hadronic properties.

Finally, as discussed in section I, experiments such as the Electron-Ion Collider [1] at Brookhaven National Laboratory and COMPASS/AMBER at CERN [2], which are designed to study hadronic structure properties, provide a great opportunity and motivation for the theoretical calculation of hadron structure on the light front.

References

[1] A. Accardi et al., "Electron Ion Collider: The Next QCD Frontier: Understanding the glue that binds us all", Eur. Phys. J. A **52**, edited by A. Deshpande, Z. E. Meziani, and J. W. Qiu, 268 (2016).

[2] B. Adams et al., "Letter of Intent: A New QCD facility at the M2 beam line of the CERN SPS (COMPASS++/AMBER)", (2018).

[3] R. W. McAllister and R. Hofstadter, "Elastic Scattering of 188-Mev Electrons from the Proton and the Alpha Particle", Phys. Rev. **102**, 851–856 (1956).

[4] G. Eichmann, *QCD and Hadron Physics Lecture Notes* (2020).

[5] H.-W. Lin et al., "Parton distributions and lattice QCD calculations: a community white paper", Prog. Part. Nucl. Phys. **100**, 107–160 (2018).

[6] K. Cichy, "Progress in x-dependent partonic distributions from lattice QCD", in 38th International Symposium on Lattice Field Theory (Oct. 2021).

[7] M. Constantinou, "The x-dependence of hadronic parton distributions: A review on the progress of lattice QCD", Eur. Phys. J. A **57**, 77 (2021).

[8] T. Frederico, G. Salmè, and M. Viviani, "Quantitative studies of the homogeneous Bethe-Salpeter equation in Minkowski space", Phys. Rev. D **89**, 016010 (2014).

[9] C. L. G. Gomez, "Minkowski space Bethe-Salpeter equation within Nakanishi representation", en, PhD thesis (Universidade Estadual Paulista, Instituto de Física Teórica, 2016), p. 163.

[10] J.-L. Zhang et al., "Measures of pion and kaon structure from generalised parton distributions", Physics Letters B **815**, 136158 (2021).

[11] K. Raya et al., *Revealing pion and kaon structure via generalised parton distributions*, 2021.

[12] W. de Paula et al., "Observing the Minkowskian dynamics of the pion on the null-plane", Phys. Rev. D **103**, 014002 (2021).

[13] C. Lorce, B. Pasquini, and M. Vanderhaeghen, "Unified framework for generalized and transverse-momentum dependent parton distributions within a 3Q light-cone picture of the nucleon", JHEP **05**, 041 (2011).

[14] S. Leitão et al., "Comparison of two Minkowski-space approaches to heavy quarkonia", Eur. Phys. J. C **77**, 696 (2017).

[15] G. Eichmann et al., "Scattering amplitudes and contour deformations", Phys. Rev. D **100**, 094001 (2019).

[16] G. Eichmann et al., "Baryons as relativistic three-quark bound states", Progress in Particle and Nuclear Physics **91**, 1–100 (2016).

[17] E. E. Salpeter and H. A. Bethe, "A Relativistic Equation for Bound-State Problems", Phys. Rev. **84**, 1232–1242 (1951).

[18] F. J. Dyson, "The S Matrix in Quantum Electrodynamics", Phys. Rev. **75**, 1736–1755 (1949).

[19] J. Schwinger, "On the Green's functions of quantized fields. I", Proceedings of the National Academy of Sciences **37**, 452–455 (1951).

[20] P. A. M. Dirac, "Forms of Relativistic Dynamics", Rev. Mod. Phys. **21**, 392–399 (1949).

[21] G. C. Wick, "Properties of Bethe-Salpeter Wave Functions", Phys. Rev. **96**, 1124–1134 (1954).

[22] R. E. Cutkosky, "Solutions of a Bethe-Salpeter Equation", Phys. Rev. **96**, 1135–1141 (1954).

[23] N. Nakanishi, "Partial-Wave Bethe-Salpeter Equation", Phys. Rev. **130**, 1230–1235 (1963).

[24] W. H. Press et al., *Numerical Recipes in C, The Art of Scientific Computing*, 2nd ed. (Cambridge University Press, 1992).

[25] L. Schlessinger, "Use of Analyticity in the Calculation of Nonrelativistic Scattering Amplitudes", Phys. Rev. **167**, 1411–1423 (1968).

[26] P. Zyla et al., "Review of Particle Physics", PTEP **2020**, 083C01 (2020).